out epigenetic reprogramming that occurs post-fertilization (*29*, *30*). It is noteworthy that 63 of the 72 C-DMRs overlap with regions previously shown to have altered methylation patterns in methylation enzyme mutants (Fig. 4) (*3*). Of the 14 C-DMRs that overlap with genes, 5 become reexpressed in *met1-3* and 1 transcript becomes silenced in *rdd* (*3*). These results suggest that a failure to faithfully maintain genome-wide methylation patterns by *MET1* and/or *RDD* is likely one source of spontaneous epiallele formation.

Regardless of their origin, the majority of epialleles identified in this study are meiotically stable and heritable across many generations in this population. Understanding the basis for such transgenerational instability and the mechanism(s) that trigger and/or release these epiallelic states will be of great importance for future studies.

References and Notes

1. J. A. Law, S. E. Jacobsen, *Nat. Rev. Genet.* **11**, 204 (2010).
2. S. J. Cokus *et al.*, *Nature* **452**, 215 (2008).
3. R. Lister *et al.*, *Cell* **133**, 523 (2008).
4. X. Zhang *et al.*, *Cell* **126**, 1189 (2006).
5. D. Zilberman, M. Gehring, R. K. Tran, T. Ballinger, S. Henikoff, *Nat. Genet.* **39**, 61 (2007).
6. S. W.-L. Chan *et al.*, *Science* **303**, 1336 (2004).
7. J. Paszkowski, U. Grossniklaus, *Curr. Opin. Plant Biol.* **14**, 195 (2011).
8. E. J. Richards, *Nat. Rev. Genet.* **7**, 395 (2006).
9. K. Shibuya, S. Fukushima, H. Takatsuji, *Proc. Natl. Acad. Sci. U.S.A.* **106**, 1660 (2009).
10. P. Cubas, C. Vincent, E. Coen, *Nature* **401**, 157 (1999).
11. K. Manning *et al.*, *Nat. Genet.* **38**, 948 (2006).
12. A. J. Thompson *et al.*, *Plant Physiol.* **120**, 383 (1999).
13. M. W. Vaughn *et al.*, *PLoS Biol.* **5**, e174 (2007).
14. F. Johannes *et al.*, *PLoS Genet.* **5**, e1000530 (2009).
15. F. K. Teixeira *et al.*, *Science* **323**, 1600 (2009); 10.1126/science.1165313.
16. A. Vongs, T. Kakutani, R. A. Martienssen, E. J. Richards, *Science* **260**, 1926 (1993).
17. R. G. Shaw, D. L. Byers, E. Darmo, *Genetics* **155**, 369 (2000).
18. S. Ossowski *et al.*, *Science* **327**, 92 (2010).
19. Additional experiments and descriptions of methods used to support our conclusions are presented as supporting material on *Science* Online.
20. C. M. Nievergelt *et al.*, *Am. J. Med. Genet. B. Neuropsychiatr. Genet.* **141B**, 234 (2006).
21. M. A. Zapala, N. J. Schork, *Proc. Natl. Acad. Sci. U.S.A.* **103**, 19430 (2006).
22. R. K. Chodavarapu *et al.*, *Nature* **466**, 388 (2010).
23. J. Liu, Y. He, R. Amasino, X. Chen, *Genes Dev.* **18**, 2873 (2004).
24. J. Bender, G. R. Fink, *Cell* **83**, 725 (1995).
25. S. Melquist, B. Luff, J. Bender, *Genetics* **153**, 4017 (1999).
26. S. E. Jacobsen, E. M. Meyerowitz, *Science* **277**, 1100 (1997).
27. H. Saze, T. Kakutani, *EMBO J.* **26**, 3641 (2007).
28. W. J. Soppe *et al.*, *Mol. Cell* **6**, 791 (2000).
29. R. A. Mosher *et al.*, *Nature* **460**, 283 (2009).
30. R. K. Slotkin *et al.*, *Cell* **136**, 461 (2009).

Acknowledgments: We thank M. White, R. Lister, M. Galli, and R. Amasino for discussions; R. Shaw and E. Darmo for seeds; J. Nery for sequencing operations; and M. Axtell for Southern blot protocol. R.J.S. was supported by an NIH National Research Service Award postdoctoral fellowship (F32-HG004830). M.D.S. was supported by a NSF Integrative Graduate Education and Research Traineeship grant (DGE-0504645). M.G.L. was supported by an European Union Framework Programme 7 Marie Curie International Outgoing Fellowship (project 252475). O.L. and N.J.S. are supported by NIH/National Center for Research Resources grant number UL1 RR025774. This work was supported by the Mary K. Chapman Foundation, the NSF (grants MCB-0929402 and MCB1122246), the Howard Hughes Medical Institute, and the Gordon and Betty Moore Foundation (GBMF) to J.R.E. J.R.E. is a HHMI–GBMF Investigator. Analyzed data sets can be viewed at http://neomorph.salk.edu/30_generations/browser.html. Sequence data can be downloaded from National Center for Biotechnology Information Sequence Read Archive (SRA035939). Correspondence and requests for materials should be addressed to J.R.E. (ecker@salk.edu).

Supporting Online Material

www.sciencemag.org/cgi/content/full/science.1212959/DC1
Materials and Methods
SOM Text
Figs. S1 to S11
Tables S1 to S16
References

22 August 2011; accepted 7 September 2011
Published online 15 September 2011;
10.1126/science.1212959

Computation-Guided Backbone Grafting of a Discontinuous Motif onto a Protein Scaffold

Mihai L. Azoitei,[1]* Bruno E. Correia,[1,2]* Yih-En Andrew Ban,[1]† Chris Carrico,[1,3] Oleksandr Kalyuzhniy,[1] Lei Chen,[4] Alexandria Schroeter,[1] Po-Ssu Huang,[1] Jason S. McLellan,[4] Peter D. Kwong,[4] David Baker,[1,5] Roland K. Strong,[3] William R. Schief[1,6,7]‡

The manipulation of protein backbone structure to control interaction and function is a challenge for protein engineering. We integrated computational design with experimental selection for grafting the backbone and side chains of a two-segment HIV gp120 epitope, targeted by the cross-neutralizing antibody b12, onto an unrelated scaffold protein. The final scaffolds bound b12 with high specificity and with affinity similar to that of gp120, and crystallographic analysis of a scaffold bound to b12 revealed high structural mimicry of the gp120-b12 complex structure. The method can be generalized to design other functional proteins through backbone grafting.

Computational protein design tests our understanding of protein structure and folding and provides valuable reagents for biomedical and biochemical research; long-term goals include the design of field- or clinic-ready biosensors (*1*), enzymes (*2*), therapeutics (*3*), and vaccines (*4*, *5*). A major limitation has been an inability to manipulate backbone structure; most computational protein design has involved sequence design on predetermined backbone structures or with minor backbone movement (*1*–*5*). Accurate backbone remodeling presents a substantial challenge for computational methods owing to limited conformational sampling and imperfect energy functions (*6*).

Novel recognition modules (*7*), inhibitors (*8*, *9*), enzymes (*2*), and immunogens (*4*, *5*, *10*, *11*) have been designed by grafting functional constellations of side chains onto protein scaffolds of predefined backbone structure. In all cases, the restriction to using predetermined scaffold backbone structures limited the complexity of the functional motifs that could be transplanted. For example, the de novo enzymes could accommodate grafting of only three or four catalytic groups, whereas many natural enzymes have six or more (*12*), and the immunogens were limited to continuous (single-segment) epitopes even though most antibody epitopes are discontinuous (involving two or more antigen segments) (*13*, *14*).

To address the challenge of incorporating backbone flexibility modeling into grafting design, we developed a hybrid computational-experimental method for grafting the backbone and side chains of functional motifs onto scaffolds (Fig. 1). We tested this method by grafting a discontinuous HIV gp120 epitope, targeted by the broadly neutralizing monoclonal antibody b12 (*15*), onto an unrelated scaffold. b12 binds to a conserved epitope within the CD4-binding site (CD4bs) of gp120 (*16*), an area of great interest for vaccine design. We focused on transplantation of two segments from gp120: residues 365 to 372, known as the CD4b (CD4 binding) loop (*17*), and residues 472 to 476, known as the ODe (outer domain exit) loop (*16*). The b12-gp120 interaction involves six or seven backbone segments on gp120 (*16*), but 60% of the buried surface area on gp120 lies on the CD4b and ODe loops, and a Rosetta energy calculation (*18*) suggested that these two

[1]Department of Biochemistry, University of Washington, Seattle, WA 98195, USA. [2]Ph.D. Program in Computational Biology, Instituto Gulbenkian de Ciência, Oeiras, Portugal. [3]Divison of Basic Sciences, Fred Hutchinson Cancer Research Center, Seattle, WA 98109, USA. [4]Vaccine Research Center, National Institute of Allergy and Infectious Diseases, Bethesda, MD 20892, USA. [5]Howard Hughes Medical Institute, University of Washington, Seattle, WA 98195, USA. [6]IAVI Neutralizing Antibody Center, The Scripps Research Institute, La Jolla, CA 92037, USA. [7]Department of Immunology and Microbial Science, The Scripps Research Institute, La Jolla, CA 92037, USA.

*These authors contributed equally to this work.
†Present address: Arzeda Corporation, Seattle, WA 98102, USA.
‡To whom correspondence should be addressed. E-mail: schief@scripps.edu

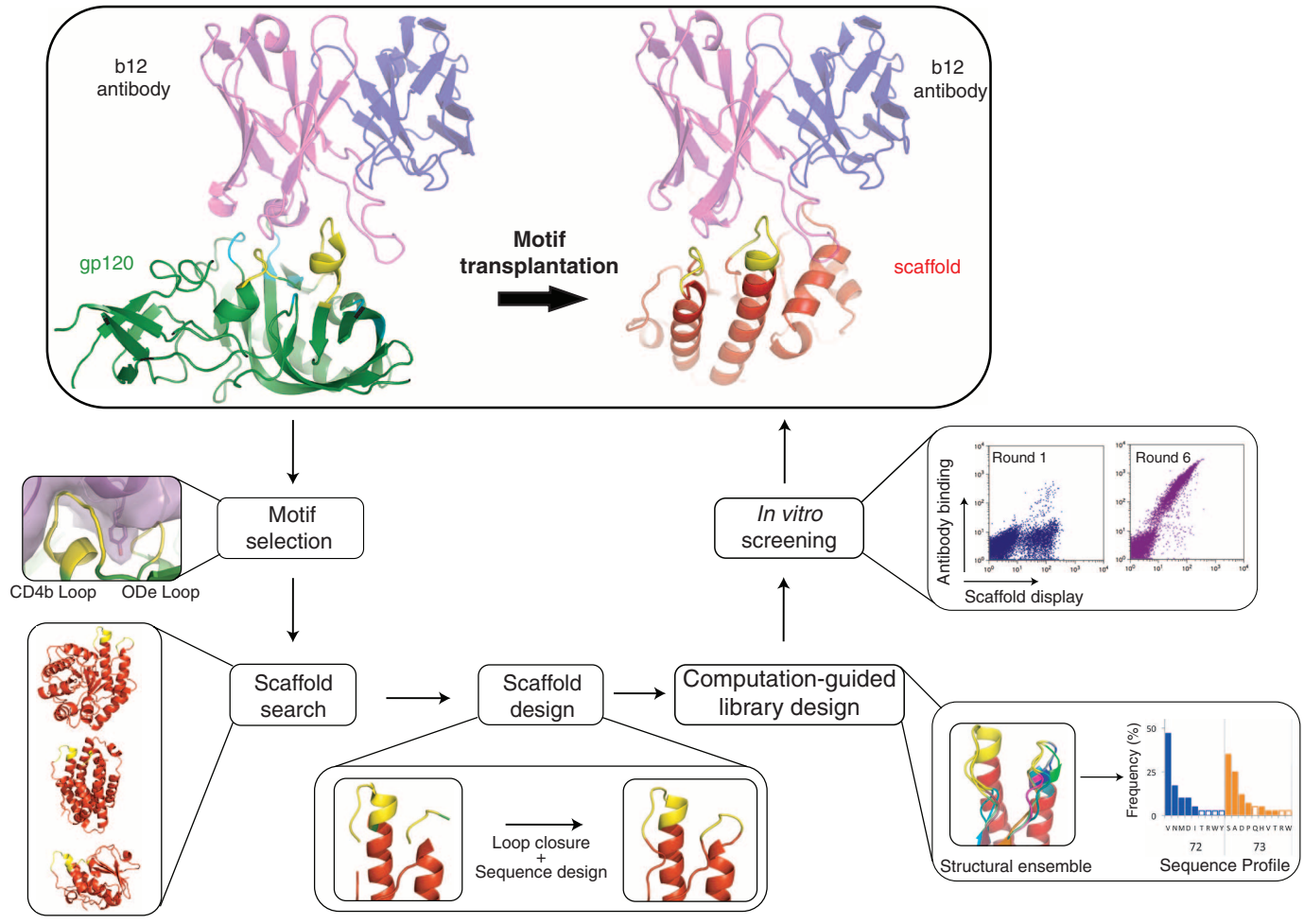

Fig. 1. Combined in silico–in vitro strategy for the transplantation of complex structural motifs to heterologous scaffold proteins. The diagrams illustrate the stages in the design of a non-HIV scaffold presenting two loops from the b12 epitope on HIV gp120.

segments could account for up to 80% of the binding energy.

The work flow (Fig. 1) has four stages: (i) scaffold search, in which the Protein Data Bank (PDB) (*19*) is searched for scaffolds suitable to accept the backbone segments comprising the motif; (ii) scaffold design, in which the motif backbone segments replace native scaffold backbone and new connecting segments and surrounding side chains are built to support the motif conformation; (iii) computation-guided library design, in which a small set of mutagenesis libraries for sequential screening are derived from an ensemble of designs with expanded structural and compositional diversity in the connecting segments; and (iv) in vitro screening, in which computation-guided libraries are screened to identify clones with optimal functional activity.

For scaffold search, we developed an algorithm (Multigraft Match) that exhaustively searched a culled PDB for suitable scaffolds. For all possible combinations of four insert positions in every scaffold, Multigraft Match produced a low-resolution prediction of whether the epitope backbone segments could be grafted onto the scaffold while maintaining backbone continuity and avoiding steric clash (fig. S1). Eleven scaffolds satisfied the geometrical and steric clash requirements and were selected for design (table S1).

For scaffold design, we developed an algorithm (Multigraft Design) that, given a preliminary rigid-body orientation for a discontinuous epitope relative to a scaffold, deleted appropriate regions of the scaffold, built new segments to connect the epitope to the scaffold, and designed side chains neighboring the epitope and connecting segments to support the graft (fig. S2). This involved aggressive structural manipulations, including replacement of ordered secondary structure motifs by the epitope segments, flexible backbone modeling of two or more connecting segments, and sequence design of 10 or more core residues. Several design variants of each candidate scaffold (fig. S3) were tested for expression and purification in *Escherichia coli*. Of 62

Table 1. Affinity and kinetics of the interaction between recombinant 2bodx variants and b12. For all the reported values, the standard error is ≤ ±7 of the last significant digit. RL, random library; L1, library 1; L2, library 2; L3, library 3. k_{on} and k_{off} represent the kinetic association and dissociation rates, respectively, of the measured interactions.

2bodx variant	Origin	b12 interaction parameters (SPR)			
		k_{on} (M^{-1} s^{-1})	k_{off} (s^{-1})	K_D (kinetic) (nM)	K_D (equilibrium) (nM)
03	Initial design				$>300 \times 10^3$
Y3	RL				$\sim 30 \times 10^3$
42	L1 + L2	1.3×10^6	2.3×10^{-1}	177	166.6
43	L1 + L2 + RL	3.0×10^6	1.0×10^{-1}	33.3	33.5
44	L1 + L2 + RL + L3	1.9×10^6	3.6×10^{-2}	18.9	19.5
45	L1 + L2 + RL + L3	3.8×10^6	3.9×10^{-2}	10.3	10.3

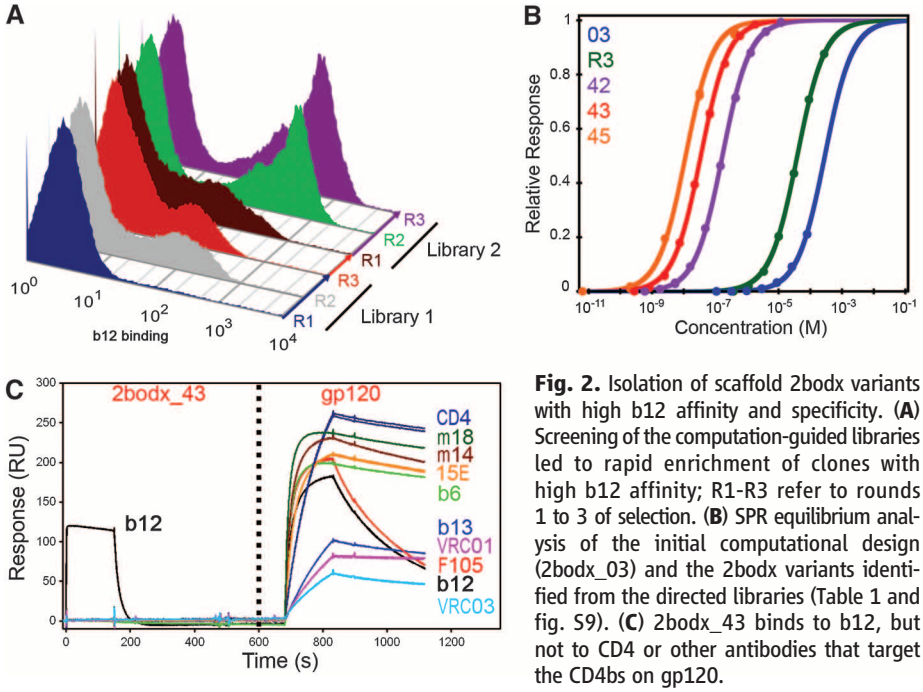

Fig. 2. Isolation of scaffold 2bodx variants with high b12 affinity and specificity. (**A**) Screening of the computation-guided libraries led to rapid enrichment of clones with high b12 affinity; R1-R3 refer to rounds 1 to 3 of selection. (**B**) SPR equilibrium analysis of the initial computational design (2bodx_03) and the 2bodx variants identified from the directed libraries (Table 1 and fig. S9). (**C**) 2bodx_43 binds to b12, but not to CD4 or other antibodies that target the CD4bs on gp120.

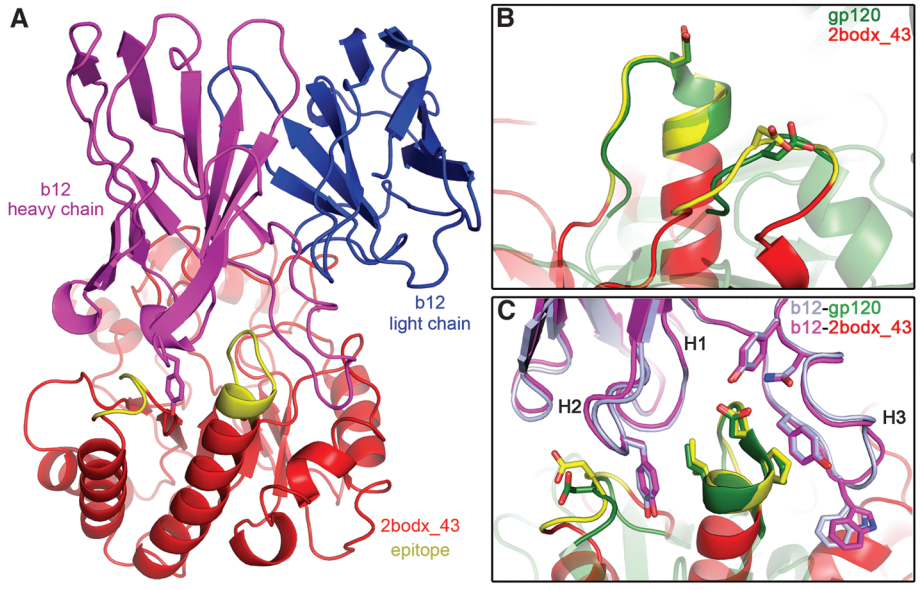

Fig. 3. Atomic-level recapitulation of the b12-gp120 interface by the b12-2bodx_43 complex. (**A**) Structure of b12 in complex with 2bodx_43. (**B**) The conformations of the transplanted loops (yellow) in 2bodx_43 (red) mimic their conformations on gp120 (green). (**C**) Conformations of side chains (sticks) making important contacts in the b12-gp120 complex are preserved at the 2bodx_43-b12 interface; H1, H2 and H3 refer to the CDR loops of b12.

candidates tested, 25 could be solubly expressed and purified (table S1).

Purified designs were tested for b12 binding by surface plasmon resonance (SPR). One design, 2bodx_03, which had 39 mutations and 11 deletions relative to the parent protein (fig. S4), bound to b12 weakly (dissociation constant $K_D \approx$ 300 μM). The binding was specific, because no binding was detected for the epitope mutant $Asp^{114} \rightarrow$ Arg (D114R) (*20*) (fig. S5). A high-resolution (1.3 Å) crystal structure of 2bodx_03 showed no discernible electron density for the epitope or connecting segments (fig. S5 and table S2), indicating that these regions were flexible in solution. In an initial attempt to optimize the b12 affinity of 2bodx_03, a whole-protein random mutagenesis library was screened by yeast display (*21*). Clone 2bodx_R3 was thereby isolated with two mutations [$Ser^{177} \rightarrow$ Gly (S177G) and $Ala^{118} \rightarrow$ Val (A118V)] from 2bodx_03 and a factor of 10 higher affinity for b12 ($K_D \approx 30$ μM) (Table 1, Fig. 2, and fig. S6). This interaction remained three orders of magnitude weaker than gp120-b12 interaction [$K_D = 20$ nM (*16*)]. The low affinity was likely due to nonoptimal sequences and conformations in the connecting segments. Optimization by targeted random mutagenesis and in vitro screening was not feasible because allowing 20 amino acids at all 21 positions judged to be important in the connecting segments would yield impractical library sizes of 2×10^{27}.

In computation-guided library design, we used a structure-sequence diversification protocol (fig. S7) to devise relatively small libraries based on more complete sampling of low-energy structures and sequences in the connecting segments. For each connecting segment, 20,000 backbone conformations were separately generated and subjected to sequence design while keeping the rest of the 2bodx_03 structure fixed. Several low-energy models for each segment were exhaustively recombined in silico and subjected to further sequence design to identify 2bodx models with optimal structures and sequences in all connecting segments. After a final round of conformational resampling and design (fig. S7), the best 45 models by several Rosetta metrics (*18*) were used to generate sequence profiles to identify the amino acids that occurred at each of the 21 positions in the connecting segments (fig. S8). The diversity was reduced by eliminating residues that occurred at low frequency, that were similar in size and chemical nature to more frequent residues, or that were judged likely to bury a polar side chain. The final library allowed mutations at 21 positions and had a theoretical size of 10^{12}.

For in vitro screening, we used yeast display. To overcome the limitations of the library size supported by yeast display (10^7), we constructed two partially overlapping sublibraries and screened them sequentially (figs. S9 and S10). The first sublibrary (library 1) contained all (4×10^6) of the computationally designed ODe loop connecting segments combined with eight design variants of the CD4b loop connecting segments present in 23 of the 45 models. After three rounds of screening, the selected ODe loop variants (from at least 18 different clones) were combined with all (2×10^5) of the computationally designed CD4b loop variants to create library 2. This sublibrary was screened for three rounds to isolate clone 2bodx_42, which differed from 2bodx_03 by 17 mutations (fig. S11). Recombinant 2bodx_42 bound b12 with a K_D of 166 nM, an improvement by a factor of >1800 over 2bodx_03 (Table 1). Introducing the A118V mutation from 2bodx_R3 further increased b12 affinity, as the resulting variant (2bodx_43) bound b12 with a K_D of 33 nM (Table 1, Fig. 2, and fig. S6), within a factor of 2 of the b12-gp120 affinity (*16*). Introducing the D114R mutation on 2bodx_43 resulted in loss of detectable b12 binding (fig. S12), demonstrating that the binding was specific to the epitope. Further, 2bodx_43 was thermally stable (melting point = 75°C) and monomeric in solution (fig. S13).

To assess whether the b12 affinity could be improved further and to evaluate if the computation-

guided libraries restricted the sequence space effectively, we screened a third library based on 2bodx_43 with expanded sampling at seven positions (fig. S10). The highest-affinity clone isolated (2bodx_45) differed from 2bodx_43 by two mutations (fig. S4) and bound b12 with a K_D of 10 nM, a factor of 3 better than 2bodx_43 and as tightly as gp120 (*16*) (Table 1, Fig. 2, and fig S6). Another high-affinity variant selected from this library (2bodx_44, K_D = 19 nM, fig. S6) was used to investigate the b12 binding contributions of library-selected mutations. We measured the b12 binding of 2bodx_44 constructs in which the "evolved" residues were individually reverted to their 2bodx_03 identity. Only 6 of 16 reversions reduced the b12 affinity of 2bodx_44 by a factor of 3 or more, and a 2bodx_03 variant that contained nine of the 2bodx_44 mutations had only micromolar affinity for b12 (K_D = 1.5 μM) (fig. S14). Thus, the selected mutations made synergistic contributions to the high b12 affinity of 2bodx constructs.

To evaluate the degree to which the 2bodx-b12 interaction recapitulated the gp120-b12 interaction, we solved a crystal structure for 2bodx_43 complexed with b12 at 2.07 Å resolution (Fig. 3A and table S2). Comparison with the gp120-b12 complex (*16*) revealed a high degree of mimicry; superposition of the epitope and paratope of both complexes gave an overall backbone root mean square deviation (RMSD) of 0.71 Å (Fig. 3, B and C) (*22*). Consistent with good backbone mimicry, important interactions involving b12 heavy-chain residues Tyr^{53}, Tyr^{98}, Trp^{100}, Asn^{100g}, and Tyr^{100h} were recapitulated in the 2bodx_43-b12 complex (Fig. 3C and tables S3 and S4). The total buried areas in the complexes were also similar, except for a small additional area on the scaffold outside the epitope (fig. S15).

The CD4bs is a major antibody target in HIV infection (*23*). Reagents are desired that bind b12 but not CD4bs-directed non-neutralizing antibodies (*24*) such as b13 that engages gp120 similarly to b12 (*25*). Of eight CD4bs-directed antibodies tested, 2bodx_43 bound tightly to b12 only (Fig. 2C). Additional SPR analyses showed that 2bodx_43 binds more tightly to b12 than to b13 by a factor of >10,000 (fig. S16) (*26*). These results indicate that b12 epitope-scaffolds are promising tools for HIV vaccine research and encourage the application of backbone grafting to engineer antigens, enzymes, and inhibitors.

References and Notes

1. L. L. Looger, M. A. Dwyer, J. J. Smith, H. W. Hellinga, *Nature* **423**, 185 (2003).
2. J. B. Siegel *et al.*, *Science* **329**, 309 (2010).
3. S. J. Fleishman *et al.*, *Science* **332**, 816 (2011).
4. B. E. Correia *et al.*, *Structure* **18**, 1116 (2010).
5. G. Ofek *et al.*, *Proc. Natl. Acad. Sci. U.S.A.* **107**, 17880 (2010).
6. D. J. Mandell, T. Kortemme, *Nat. Chem. Biol.* **5**, 797 (2009).
7. S. E. Rutledge, H. M. Volkman, A. Schepartz, *J. Am. Chem. Soc.* **125**, 14336 (2003).
8. S. K. Sia, P. S. Kim, *Proc. Natl. Acad. Sci. U.S.A.* **100**, 9756 (2003).
9. L. Martin *et al.*, *Nat. Biotechnol.* **21**, 71 (2002).
10. E. Drakopoulou *et al.*, *J. Biol. Chem.* **271**, 11979 (1996).
11. S. M. Lu, R. S. Hodges, *J. Biol. Chem.* **277**, 23515 (2002).
12. D. Baker, *Protein Sci.* **19**, 1817 (2010).
13. L. Jin, B. M. Fendly, J. A. Wells, *J. Mol. Biol.* **226**, 851 (1992).
14. N. D. Rubinstein *et al.*, *Mol. Immunol.* **45**, 3477 (2008).
15. D. R. Burton *et al.*, *Science* **266**, 1024 (1994).
16. T. Zhou *et al.*, *Nature* **445**, 732 (2007).
17. B. Chen *et al.*, *Nature* **433**, 834 (2005).
18. See supporting material on *Science* Online.
19. H. M. Berman *et al.*, *Nucleic Acids Res.* **28**, 235 (2000).
20. Y. Li *et al.*, *Nat. Med.* **13**, 1032 (2007).
21. G. Chao *et al.*, *Nat. Protoc.* **1**, 755 (2006).
22. With the overall interface superposition of the 2bodx_43-b12 and gp120-b12 complexes, RMSD values for individual elements were low, as follows: CD4b loop, 0.8 Å; ODe loop, 1.5 Å; b12 CDRH1 residues 25 to 34, 0.28 Å; H2 residues 52 to 56, 0.6 Å; H3 residues 94 to 101, 0.7 Å.
23. L. Stamatatos, L. Morris, D. R. Burton, J. R. Mascola, *Nat. Med.* **15**, 866 (2009).
24. R. Pantophlet *et al.*, *J. Virol.* **77**, 642 (2003).
25. L. Chen *et al.*, *Science* **326**, 1123 (2009).
26. The very low affinity of b13 for 2bodx_43 is likely due to (i) the different conformations of the CD4b and ODe loops in the b13-gp120 structure compared to the b12-gp120 and b12-2bodx_43 structures, and (ii) important contacts for b13 at gp120 residues 419, 421, and 425 in the β20-β21 region not present on the scaffold.

Acknowledgments: Supported by grants from the International AIDS Vaccine Initiative Neutralizing Antibody Consortium and the Bill and Melinda Gates Foundation Consortium for AIDS Vaccine Discovery. B.E.C. was supported by a fellowship from the Portuguese Fundação para a Ciência e a Tecnologia (SFRH/774 BD/32958/2006). We thank I. Wilson for comments on the manuscript; D. Burton, A. Hessell, and the IAVI Neutralizing Antibody Consortium Reagent Repository for providing b6, b12, and b13; J. Mascola for VRC01 and VRC03; Progenics Inc. for CD4-IgG2; D. Dimitrov for m6, m14, and m18; J. Robinson for 15E; and R. Wyatt for F105 and HxB2 gp120. We thank G. Nabel, M. Kanekiyo, and Z.-Y. Yang for experiments on early generations of b12 scaffolds. Coordinates and structure factors were deposited in the PDB as entries 3RPT and 3RU8. The University of Washington has filed a patent application on the b12 scaffolds and the scaffolding method developed in this study. Materials and information will be provided to noncommercial users under the Uniform Biological Materials Transfer Agreement. The Multigraft software developed in this work is freely available to noncommercial users through the Rosetta Commons agreement (www.rosettacommons.org).

Supporting Online Material

www.sciencemag.org/cgi/content/full/334/6054/373/DC1
Materials and Methods
Figs. S1 to S16
Tables S1 to S4
References

6 June 2011; accepted 8 September 2011
10.1126/science.1209368

Antagonists Induce a Conformational Change in cIAP1 That Promotes Autoubiquitination

Erin C. Dueber,[1] Allyn J. Schoeffler,[1] Andreas Lingel,[1] J. Michael Elliott,[2] Anna V. Fedorova,[1] Anthony M. Giannetti,[3] Kerry Zobel,[1] Brigitte Maurer,[4] Eugene Varfolomeev,[1] Ping Wu,[4] Heidi J. A. Wallweber,[4] Sarah G. Hymowitz,[4] Kurt Deshayes,[1] Domagoj Vucic,[1]* Wayne J. Fairbrother[1]*

Inhibitor of apoptosis (IAP) proteins are negative regulators of cell death. IAP family members contain RING domains that impart E3 ubiquitin ligase activity. Binding of endogenous or small-molecule antagonists to select baculovirus IAP repeat (BIR) domains within cellular IAP (cIAP) proteins promotes autoubiquitination and proteasomal degradation and so releases inhibition of apoptosis mediated by cIAP. Although the molecular details of antagonist–BIR domain interactions are well understood, it is not clear how this binding event influences the activity of the RING domain. Here biochemical and structural studies reveal that the unliganded, multidomain cIAP1 sequesters the RING domain within a compact, monomeric structure that prevents RING dimerization. Antagonist binding induces conformational rearrangements that enable RING dimerization and formation of the active E3 ligase.

Inhibitor of apoptosis (IAP) proteins are anti-apoptotic factors important in blocking programmed cell death, or apoptosis, in response to a variety of stimuli (*1*, *2*). Whether initiated by external death signals transduced by specific cell surface receptors (extrinsic pathway) or by internal cues of compromised cellular integrity (intrinsic pathway), apoptotic signaling pathways converge in the activation of caspases (cysteine-dependent aspartyl-specific proteases), which effect widespread proteolytic damage and cell death (*3*). IAPs hold these cellular executioners in check, either through direct inhibitory interactions or by impeding upstream caspase activation pathways (*4*). Many cancer cells overexpress IAPs, which allows them to resist cytotoxic therapies (*2*, *5*). Thus, IAPs are potentially important targets for cancer treatment (*2*, *5*, *6*).

IAP-targeting therapeutics designed to mimic the endogenous IAP antagonist, SMAC (second mitochondrial activator of caspases)–DIABLO (direct IAP-binding protein with low isoelectric point) (*7*, *8*), have recently entered phase I clinical

[1]Department of Early Discovery Biochemistry, Genentech, 1 DNA Way, South San Francisco, CA 94080, USA. [2]Department of Protein Chemistry, Genentech, 1 DNA Way, South San Francisco, CA 94080, USA. [3]Department of Biochemical Pharmacology, Genentech, 1 DNA Way, South San Francisco, CA 94080, USA. [4]Department of Structural Biology, Genentech, 1 DNA Way, South San Francisco, CA 94080, USA.

*To whom correspondence should be addressed. E-mail: fairbro@gene.com (W.J.F.); domagoj@gene.com (D.V.)

Computation-Guided Backbone Grafting of a Discontinuous Motif onto a Protein Scaffold

Mihai L. Azoitei, Bruno E. Correia, Yih-En Andrew Ban, Chris Carrico, Oleksandr Kalyuzhniy, Lei Chen, Alexandria Schroeter, Po-Ssu Huang, Jason S. McLellan, Peter D. Kwong, David Baker, Roland K. Strong and William R. Schief

Science **334** (6054), 373-376.
DOI: 10.1126/science.1209368